Spatial focalization of pheromone/MAPK signaling triggers commitment to cell–cell fusion

Omaya Dudin,[1] Laura Merlini,[1] and Sophie G. Martin

Department of Fundamental Microbiology, University of Lausanne, CH-1015 Lausanne, Switzerland

Cell fusion is universal in eukaryotes for fertilization and development, but what signals this process is unknown. Here, we show in *Schizosaccharomyces pombe* that fusion does not require a dedicated signal but is triggered by spatial focalization of the same pheromone–GPCR (G-protein-coupled receptor)–MAPK signaling cascade that drives earlier mating events. Autocrine cells expressing the receptor for their own pheromone trigger fusion attempts independently of cell–cell contact by concentrating pheromone release at the fusion focus, a dynamic actin aster underlying the secretion of cell wall hydrolases. Pheromone receptor and MAPK cascade are similarly enriched at the fusion focus, concomitant with fusion commitment in wild-type mating pairs. This focalization promotes cell fusion by immobilizing the fusion focus, thus driving local cell wall dissolution. We propose that fusion commitment is imposed by a local increase in MAPK concentration at the fusion focus, driven by a positive feedback between fusion focus formation and focalization of pheromone release and perception.

[*Keywords*: cell–cell fusion; fertilization; MAP kinase cascade; G-protein-coupled receptor signaling; pheromone; formin; fission yeast *Schizosaccharomyces pombe*]

Supplemental material is available for this article.

Received July 7, 2016; revised version accepted September 21, 2016.

Cell fusion is a widespread process that occurs in a large variety of cell types. In somatic cells, it serves to shape tissues and organs such as muscles, bones, or the placenta in metazoans or form interconnected mycelia in fungi (Read et al. 2010). In gametes, it underlies the fertilization of all sexually reproducing species. In pathogenic fungi, this process is often tightly linked with virulence (Morrow and Fraser 2009; Ene and Bennett 2014). Cell fusion may also play important roles in regeneration and cancer (Lu and Kang 2009; Lluis and Cosma 2010). In all events of cell–cell fusion, three major conceptual steps can be defined: First, signaling occurs between the two partner cells to induce cell differentiation. Second, the cells polarize toward each other for cell–cell adhesion. Third, a fusion machinery is assembled at the cell–cell contact site for membrane merging. This machinery may be composed of two main parts: a specific actin structure that promotes membrane juxtaposition (Abmayr and Pavlath 2012) and fusogenic proteins that drive membrane fusion (Aguilar et al. 2013). In walled cells, such as fungal or plant cells, the process is further complicated because the cell wall first needs to be locally degraded while preserving cell integrity. The mechanisms underlying the cellular decision to fuse are unknown.

Conceptually, cell fusion may be initiated by diverse signals: Cell fusion may be induced upon physical engagement of transmembrane proteins, although, in walled cells, this would require proteins spanning the thickness of the cell wall. The signal may be of mechanical nature, leading to mechanical sensing of cells in contact. Support for this idea comes from the observation that imbalance in the osmotic pressure between two partner cells prevents cell fusion in *Saccharomyces cerevisiae* (Philips and Herskowitz 1997). Alternatively, it may be mediated by a chemical signal between partner cells at short range. The finding that *S. cerevisiae* cells expressing reduced levels of a-factor pheromone are specifically fusion-defective (Brizzio et al. 1996) suggests that pheromones may form such chemical signals. However, addition of exogenous pheromone to cells unable to secrete it does not restore fusion ability (Michaelis and Herskowitz 1988; Kjaerulff et al. 1994; Seike et al. 2013). Individual cells exposed to even saturating pheromone levels also do not lyse (which would result from a fusion attempt without a partner cell), suggesting that the decision to fuse requires more than a simple step increase in pheromone signaling.

[1]**These authors contributed equally to this work.**
Corresponding author: sophie.martin@unil.ch
Article is online at http://www.genesdev.org/cgi/doi/10.1101/gad.286922.116.

We investigated fusion commitment in the sexual life cycle of the fission yeast *Schizosaccharomyces pombe*. Here, fusion occurs between two haploid cells of opposite mating types, known as M (h^-) and P (h^+), to form a diploid zygote. Mating is induced by nitrogen starvation and relies on pheromone-dependent communication (Merlini et al. 2013): The P cell secretes P factor, a 23-amino-acid peptide that activates its cognate receptor, Mam2, on the M cell (Kitamura and Shimoda 1991; Imai and Yamamoto 1994). Similarly, the M cell produces M factor, a short lipid-modified peptide that is transported outside M cells by a dedicated ABC-type transporter, Mam1, and sensed by the Map3 receptor on the P cell (Davey 1992; Tanaka et al. 1993; Christensen et al. 1997). Both receptors belong to the G-protein-coupled receptor (GPCR) family and signal through the same Gα subunit, Gpa1, and a conserved MAPK cascade to amplify the transcriptional mating program initially induced by nitrogen starvation (Obara et al. 1991; Hughes et al. 1993; Neiman et al. 1993; Xu et al. 1994). This leads to, among other things, the increased expression of pheromones, Mam1 transporter, pheromone receptors, and formin Fus1, which is essential for cell fusion. Beyond transcriptional control, pheromone signaling is also interpreted locally to induce polarized growth: Pheromone secretion machineries and receptor-coupled Gα coaccumulate at polarized cortical zones that dynamically explore the cell periphery and become stabilized by pheromone stimulation (Bendezu and Martin 2013; Merlini et al. 2016). Thus, facing zones in partner cells stabilize each other, leading to cell–cell pairing. In the ensuing polarized growth that brings cells into physical contact, pheromone receptors become enriched at the tip of the cellular extension (shmoo) toward the partner cell, as also observed in other fungi (Ayscough and Drubin 1998; Hirota et al. 2001; Merlini et al. 2016). Whether pheromone–MAPK signaling also directly regulates cell fusion is not known.

Cell fusion in fungi necessitates digestion of the cell wall to bring the plasma membranes into contact. In fission yeast cells, this is achieved through assembly of the actin fusion focus, a Fus1-dependent aster of linear actin cables that focalizes the myosin V-dependent delivery of cell wall glucanases to the incipient fusion site (Dudin et al. 2015). Time-lapse imaging of the fusion focus revealed that this structure forms only in paired cells in contact, suggesting the existence of a signal at close range to trigger fusion focus assembly. Indeed, as fission yeast cells are under strong internal turgor pressure, estimated to be equivalent to that in a racing bike tire (~8 atm) (Minc et al. 2009), a fusion focus assembled too early or at the wrong place would lead to osmotic shock and cell lysis.

Here, we establish that fusion commitment is triggered by spatial focalization of the known pheromone–GPCR–MAPK signaling cascade. We show that pheromone signaling is both necessary and sufficient to induce cell fusion independently of physical cell contact and that the fusion signal is encoded not in the absolute amounts of pheromone but in its spatial organization. Concentration of pheromone release, GPCR, and MAPK signaling at the actin fusion focus results from a positive feedback loop between pheromone signaling and the actin fusion focus and induces cell fusion commitment by stabilizing the focus for local cell wall digestion. Thus, spatial reorganization of the signaling cascade underlies the decision to fuse.

Results

A diffusible signal is necessary for cell fusion

Fission yeast cells efficiently form pairs and fuse when placed in a monolayer on solid medium (Dudin et al. 2015; Vjestica et al. 2016). Similarly, homothallic yeast cells loaded in a flow chamber successfully formed zygotes in the absence of fluid flow but failed to do so in the presence of flow, which likely perturbed the formation of pheromone gradients (data not shown). To test whether the flow directly perturbed fusion in addition to earlier events during mating, we let cell pairs engage in the fusion process in the absence of flow, forming fusion foci characterized by the focal localization of type V myosin Myo52 (Dudin et al. 2015), before transiently flowing fresh medium for 10 min (Fig. 1A). Cell pairs engaged in fusion exhibited one of two distinct behaviors: Some were unperturbed by the flow and retained their fusion foci, defining a committed stage undisturbed by external flow (Fig. 1B; Supplemental Movie S1). These cells rapidly fused together (Fig. 1C). Others were uncommitted and disassembled their fusion foci, reassembling them and completing fusion with significant delay after the flow had been arrested (Fig. 1B,C; Supplemental Movie S1).

Four lines of evidence indicate that the committed pairs are more advanced in the fusion process than the uncommitted ones. First, committed cells fused faster than the average of untreated cells, indicating that commitment occurs in the later stage of the fusion process (Fig. 1C). Second, the distance between the partner cell fusion foci was significantly smaller in the committed pairs, indicating closer cell–cell engagement (Fig. 1D). Third, the fusion foci were more static in the committed pairs, as observed for late fusion pairs (Fig. 1E; Dudin et al. 2015). Fourth, the second type V myosin Myo51, which accumulates at the fusion focus late in the process (Doyle et al. 2009; Dudin et al. 2015), was detected in both cells only in committed pairs (Supplemental Fig. S1). We conclude that fusion consists of two successive stages: an early, uncommitted stage that requires an external diffusible signal and a late, committed stage. We hypothesized that pheromones represent this diffusible signal for fusion.

Autocrine cells attempt fusion in the absence of a partner cell

Any instructive fusion signal should carry sufficient information to induce the fusion process. We obtained direct evidence that pheromone signaling is sufficient to induce cell fusion by constructing autocrine cells. We replaced the coding region of the P-factor receptor Mam2 with that of the M-factor receptor Map3 at endogenous *mam2* genomic locus in M cells, yielding cells that

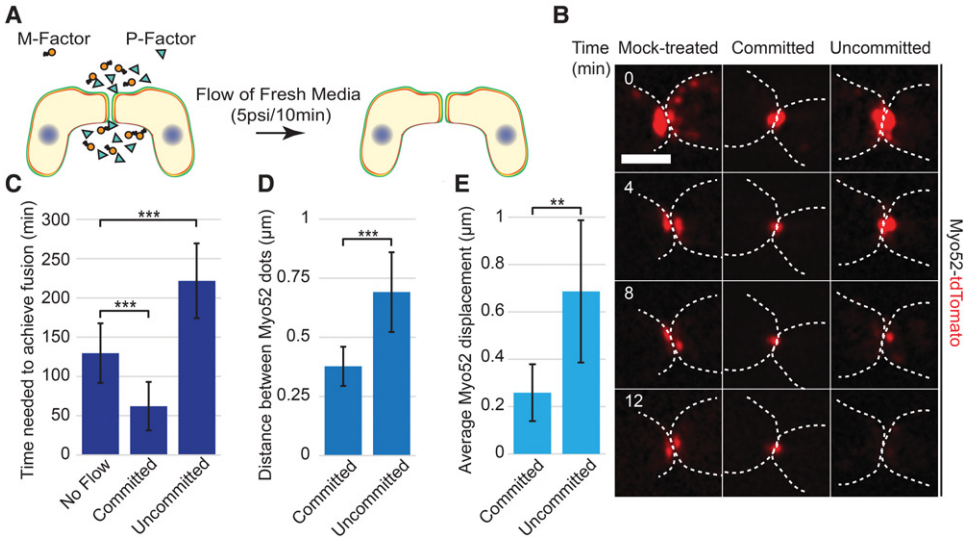

Figure 1. A diffusible signal is required for cell fusion during sexual reproduction. (*A*) Homothallic *h90* cells expressing Myo52-tdTomato and p^{map3}:GFP were loaded into CellAsic microfluidic chambers and allowed to engage in the fusion process in the absence of flow. At t_0, fresh medium was transiently flowed through the chamber for 10 min to wash out diffusible molecules, including pheromones. (*B*) Myo52-tdTomato signal in homothallic *h90* cells without (no flow) or with fresh medium flow (committed and uncommitted pairs). Committed pairs maintained their fusion focus, whereas uncommitted pairs disassembled it. Bar, 2 µm. (*C*) Time until fusion for all pairs engaged in fusion at t_0, as defined by the presence of Myo52 foci. $n > 10$. (***) $P < 4 \times 10^{-5}$, *t*-test. (*D*) Distance between Myo52-tdTomato dots at t_0. $n > 15$. (***) $P < 2 \times 10^{-7}$, *t*-test. (*E*) Mean Myo52-tdTomato displacement per 2-min time point over 12 min after t_0. $n = 9$ cells. (**) $P < 3 \times 10^{-4}$, *t*-test.

respond to the self-produced M factor (Fig. 2A). During exponential growth, autocrine M cells (*h⁻mam2Δ::map3*) were indistinguishable from wild-type M cells, as judged by cell length, cell width, septum position, growth assays, and localization of polarity factors such as type V myosin Myo52 and Cdc42 scaffold Scd2 (Supplemental Fig. S2A–E). This is consistent with the previous observations that expression of pheromones and their receptors is induced by starvation (Kitamura and Shimoda 1991; Tanaka et al. 1993; Kjaerulff et al. 1994). In contrast, upon nitrogen starvation, these autocrine cells spontaneously activated pheromone signaling, as reported previously (Tanaka et al. 1993): They stopped dividing and expressed pheromone-responsive gene products such as the pheromone transporter Mam1, the pheromone-dependent formin Fus1, and the replaced pheromone receptor Map3 (Supplemental Fig. S2F; Petersen et al. 1995; Christensen et al. 1997). Autocrine cells also exhibited strong morphological responses characteristic of sexual differentiation, forming multiple successive projections, leading to aberrantly shaped cells (Fig. 2B; Supplemental Fig. S2G). Remarkably, nearly 40% of autocrine M cells also spontaneously lysed, suggesting that these cells were mounting a fusion response in the absence of a partner cell (Fig. 2C).

To determine whether autocrine M-cell lysis was due to a genuine fusion attempt, we monitored the localization of components of the fusion focus. Myo52-tdTomato formed a tight spot in most of the autocrine M cells. Time-lapse imaging showed this spot dynamically localized at the cell cortex at zones of active cell growth (Fig. 2B; Supplemental Movie S2) as well as at sites of lysis (Fig. 2D; Supplemental Movie S2). We note that Myo52 spots associated with lysis were stable for a significantly longer time preceding the lysis event than at other times (Fig. 2E). The Myo52 spot colocalized with the formin Fus1 as well as with Exg3 and Eng2, two glucanases that localize at the fusion focus and are needed to degrade the cell wall during fusion (Fig. 2F; Dudin et al. 2015), suggesting that these led to local cell wall digestion. In agreement with this, osmotic stabilization by addition of 1.2 M sorbitol in the medium efficiently suppressed cell lysis (Fig. 2C). Finally, deletion of *fus1* prevented formation of the Myo52 focus and completely suppressed cell lysis (Fig. 2C,G; data not shown). We conclude that autocrine M cells assemble a fusion focus-like structure and attempt fusion in the absence of a partner cell, leading to cell lysis.

This attempted fusion upon autocrine signal activation represents a complete fusion response. Indeed, two autocrine M cells were occasionally able to fuse with each other. This mostly happened shortly after cell division, with the two sister cells re-fusing together (Fig. 2H; Supplemental Movie S3). While these events were infrequent, their existence demonstrates that autocrine M cells mount a genuine fusion response able to go to completion.

In summary, these data establish that the signal to trigger cell fusion does not rely strictly on cell–cell contact and can be elicited by simple autocrine activation of pheromone signaling. We infer that paracrine pheromone signaling in the normal situation of cell pair engagement also triggers fusion.

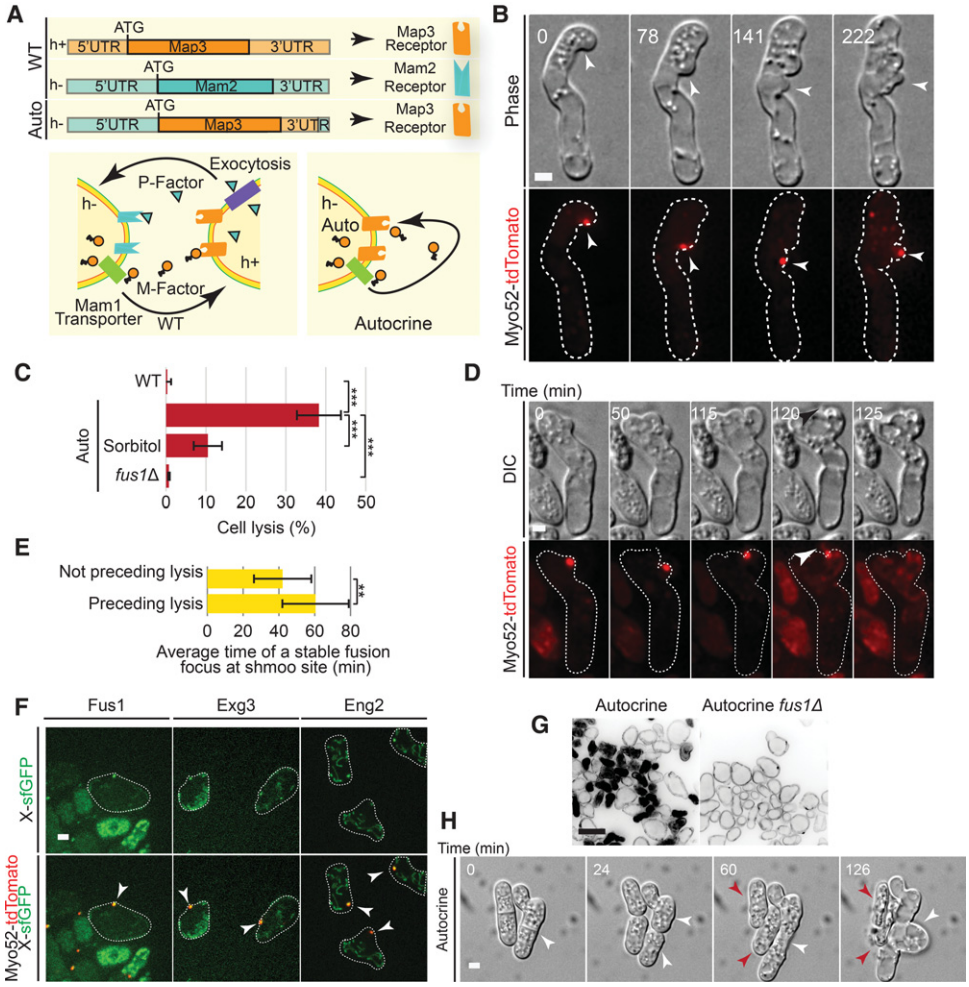

Figure 2. Autocrine cells attempt cell fusion. (*A*) Autocrine M cells (Auto) were constructed by replacing the ORF and part of the 3′ untranslated region (UTR) of *mam2* with the corresponding sequences of *map3*, encoding the M-factor receptor. Autocrine M cells thus respond to the self-produced M factor. (*B*) Autocrine cells forming several successive projections over time with a Myo52-tdTomato dot as a proxy for fusion focus localization. (*C*) Cell lysis of wild-type M cells, autocrine M cells, and autocrine M cells treated with 1.2 M sorbitol or lacking *fus1* (*fus1*Δ) after 16 h in MSL − N. $n > 1000$. (***) $P < 3 \times 10^{-4}$, *t*-test auto; (***) $P < 2 \times 10^{-5}$, *t*-test, sorbitol and *fus1*Δ. (*D*) Differential interference contrast (DIC) and Myo52-tdTomato signal in autocrine M cells. Arrowheads indicate cytosolic extrusion upon cell lysis. (*E*) Time before lysis during which the fusion focus is immobile in lysing autocrine M cells compared with the maximal length of time a focus is immobile in nonlysing autocrine M cells. $n = 15$. (**) $P < 0.01$, *t*-test. (*F*) The formin Fus1-sfGFP and cell wall glucanases Exg3-sfGFP and Eng2-sfGFP colocalize with Myo52-tdTomato at the fusion focus in autocrine M cells. (*G*) Calcofluor-stained autocrine *fus1*$^+$ and *fus1*Δ M cells. Calcofluor strongly stains dead cells. Bar, 10 µm. (*H*) DIC time-lapse image of autocrine M cells showing fusion of sister cells to create a diploid (white arrowheads), while other cells lyse (red arrowheads). Bar (except in *G*), 2 µm. Time is in minutes.

Focalized pheromone release serves as fusion signal

Addition of synthetic pheromone to heterothallic cells has been shown to promote cell cycle arrest, initiation of the sexual transcriptional program, and cell polarization (Davey and Nielsen 1994; Imai and Yamamoto 1994; Petersen et al. 1995; Christensen et al. 1997; Bendezu and Martin 2013). However, in contrast to the autocrine situation presented above, in either P or M cells exposed to very high concentrations of synthetic M or P factor, respectively, we did not observe fusion focus assembly or extensive cell lysis even upon deletion of the proteases that normally degrade these pheromones (Fig. 3A; Supplemental Fig. S3). Using time-lapse microscopy, we found that these cells transiently concentrated the Myo52 signal, but such foci were not maintained over time (L Merlini, unpubl.). One reason for this difference may be that the spatial organization of the pheromone signal is distinct in the two cases.

While pheromones are homogeneously distributed upon exogenous addition, local release in the autocrine situation may allow for a sharp, graded pheromone distribution. Although direct visualization of M factor is not possible, we found that, in autocrine M cells, the M-factor transporter Mam1 was focalized to a single sharp dot, which colocalized with the

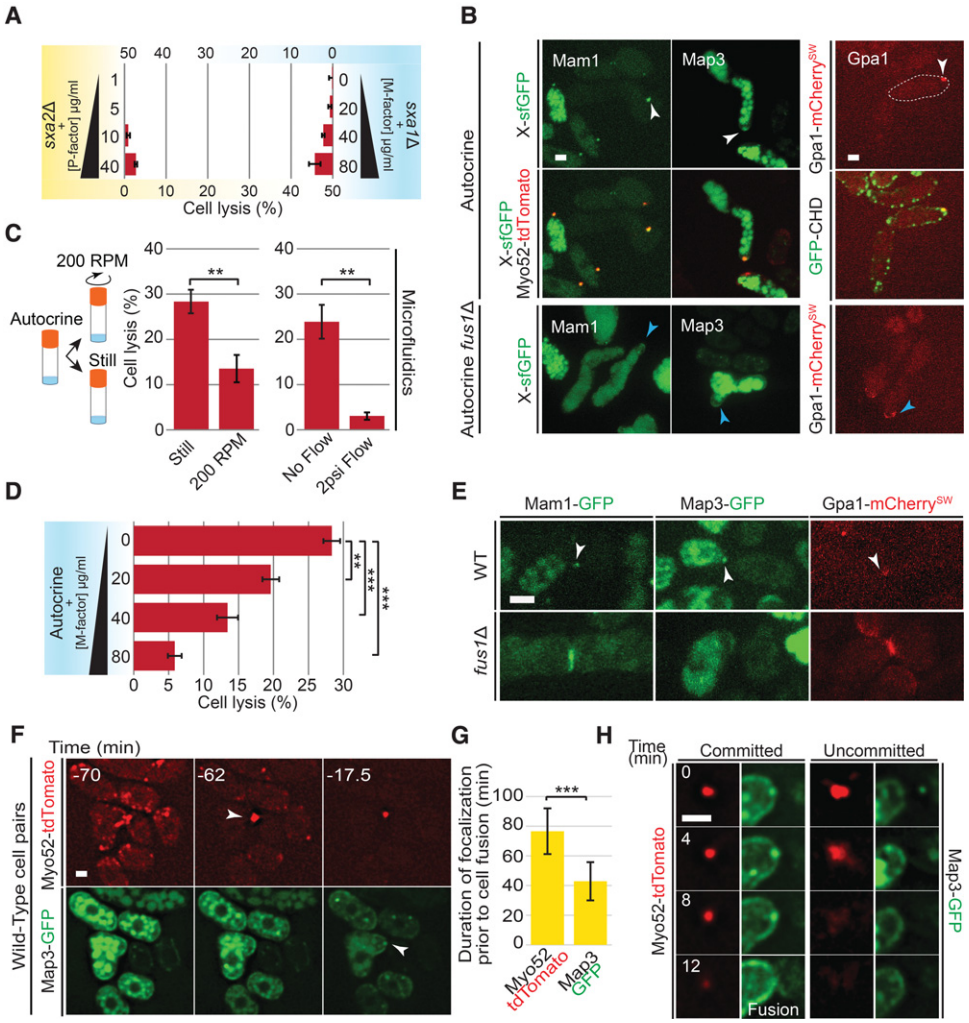

Figure 3. The pheromone release and signaling machineries focalize at the fusion site. (*A*) Addition of synthetic pheromone does not cause extensive cell lysis. Percentage of cell lysis of heterothallic h^- *sxa2*Δ and h^+ *sxa1*Δ cells 14 h after synthetic P-factor or M-factor addition, respectively. (*B*) Localization in autocrine M cells of Mam1-sfGFP, Map3-sfGFP, and Gpa1-mCherry (white arrowheads) at the fusion focus labeled with Myo52-tdTomato or GFP-CHD and over a broader region in *fus1*Δ (blue arrowheads). Note that many cells also show a strong vacuolar signal, likely due to internalization of the transporter and receptor. (*C*) Equalizing pheromone concentrations suppresses the lysis of autocrine M cells. The percentage of cell lysis is shown in liquid cultures for 16 h with or without agitation (*left*; 200 rpm; $n > 800$; [**] $P < 0.007$, *t*-test) and in microfluidic chambers for 6 h with or without flow (*right*; $n > 1000$; [**] $P < 0.008$, *t*-test). (*D*) Cell lysis of autocrine M cells after 16 h on MSL – N agarose pads supplemented with synthetic M factor at the indicated concentrations. $n > 700$. (**) $P < 0.002$; (***) $P < 5 \times 10^{-4}$, *t*-test. (*E*) Localization of Mam1-sfGFP, Map3-sfGFP, and Gpa1-mCherry at the fusion focus in wild-type mating pairs and over a broader region in *fus1*Δ. (*F*) Time lapse of Myo52-tdTomato and Map3-sfGFP in homothallic wild-type pairs. Note that Myo52-tdTomato forms a tight focus earlier than Map3 (arrowheads). t_0 is the fusion time. (*G*) Time before fusion during which the indicated signal is focalized. $n = 10$. (***) $P < 2 \times 10^{-4}$, *t*-test. (*H*) Map3-sfGFP and Myo52-tdTomato in wild-type committed and uncommitted pairs in microfluidics washed with fresh medium as in Figure 1. Map3-sfGFP focalizes with Myo52-tdTomato only in the committed pair (committed pairs: five of five; uncommitted: 10 of 10). Note that this committed pair fuses at t_{12}. Time is in minutes. Bars, 2 μm.

fusion focus (60 of 80 cells) and depended on *fus1*, suggesting that M factor is locally released at this location (Fig. 3B). Thus, autocrine activation of pheromone signaling promotes the focal organization of pheromone release.

We tested the importance of focal pheromone release to promote fusion attempts in autocrine M cells by homogenization of pheromone distribution. Autocrine M cells in suspension underwent lysis as described on solid medium above, but the number of lysed cells was reduced by strong agitation (Fig. 3C). Similarly, autocrine M cells placed in flow chambers lysed in the absence of flow but did not upon continuous flow of fresh medium (Fig. 3C). Remarkably, addition of a high concentration of M factor on solid medium also strongly reduced the occurrence of lysis (Fig. 3D), indicating that the local

pheromone gradient rather than the absolute pheromone concentration acts as fusion signal.

Pheromone signaling is focalized at the fusion focus

In addition to the Mam1 transporter, the M-factor receptor Map3 was highly enriched at the fusion focus of autocrine M cells labeled with Myo52-tdTomato (41 of 83 cells). Similarly, the receptor-coupled Gα Gpa1 localized at the fusion focus (19 of 54 cells). In *fus1*Δ autocrine cells, Map3 and Gpa1 were broadly distributed at the plasma membrane (Fig. 3B). In contrast, neither pheromone receptor (the P-factor receptor Mam2 in M cells or the M-factor receptor Map3 in P cells) was focalized in heterothallic cells exposed to a high concentration of synthetic pheromones (Supplemental Fig. S3).

This focalized organization of pheromone signaling was also observed in wild-type mating pairs: Mam1, Map3, and Gpa1 all accumulated at the fusion focus in a *fus1*-dependent manner (Fig. 3E). Time-lapse examination of Map3 showed that signaling focalization occurs late in the fusion process: Whereas Myo52 focalized 75 min ± 15 min before cell–cell fusion, Map3-GFP colocalized as a dot only 43 min ± 13 min before fusion (Fig. 3F,G). Moreover, we found that committed cells as defined in flow cell experiments (see Fig. 1) showed focalization of the pheromone receptor Map3, whereas no focalization of Map3 was observed in uncommitted cells (Fig. 3H). We conclude that pheromone signaling becomes highly spatially constrained at the fusion focus and that this correlates with commitment to cell fusion.

Loss of pheromone receptor focalization correlates with fusion defect

To test the role of pheromone signaling focalization in cell fusion, we strove to perturb signaling focalization without disturbing the formation of the fusion focus or earlier events of cell differentiation and polarization. We reasoned that the focal distribution of the transmembrane receptor would be disturbed by interfering with its endocytic retrieval, likely necessary to counter the effects of lateral diffusion at the plasma membrane. Indeed, a Map3 allele with a truncation of its C-terminal cytoplasmic tail (Map3^{dn9}-GFP, previously shown to be endocytosis-deficient) (Hirota et al. 2001) decorated the plasma membrane broadly and was not enriched at the Myo52-labeled fusion focus, whether it was expressed as the sole Map3 copy in autocrine M cells or mating P cells (Fig. 4A,B). Remarkably, the *map3^{dn9}* truncation completely blocked cell lysis in autocrine M cells (Fig. 4C). However, these cells, like their *map3^{+}* counterparts, activated pheromone signaling: They stopped dividing, expressed pheromone-responsive transcripts (data not shown), and exhibited growth projections characteristic of sexual differentiation, which, however, occurred only at cell poles (Fig. 4B). Consistently, *map3^{dn9}* mutant P cells were able to engage in mating pairs (Bendezu and Martin 2013) but were almost completely fusion-defective (Fig. 4D). Thus, the endocytosis-deficient Map3^{dn9} allele largely separates early cell differentiation and polarization events from late ones depending on focalization. We note that Map3 C-terminal truncation may also affect other aspects of its regulation in addition to endocytosis. In both autocrine cells and cell pairs, the focalization of Myo52 indicates that *map3^{dn9}* mutant cells were able to form a fusion focus (Fig. 4A,B). However, this focus was significantly more mobile than in wild-type cells (Fig. 4A,B,E; Supplemental Movie S4). As a result, glucanases failed to become enriched at a focal point (Fig. 4H). We conclude that pheromone receptor endocytosis is necessary for receptor concentration at the fusion focus and is required to stabilize the fusion focus.

We found a second condition in which the pheromone receptor is not enriched at the fusion focus by examining the phenotype of *rgs1*Δ cells. Rgs1 is a GTPase-activating protein for the receptor-coupled Gα Gpa1 previously characterized for its role in desensitization (Watson et al. 1999; Pereira and Jones 2001; Croft et al. 2013). In this mutant, which mounts an exaggerated pheromone response, the Map3 receptor was not enriched at the fusion focus in both autocrine M cells and P cells engaged in cell pairs (Fig. 4F,G). Mam1 and Gpa1 were also not enriched at the fusion site in these cells (Fig. 4G). Similar to the case of *map3^{dn9}*, *rgs1*Δ autocrine M cells did not lyse, and engaged *rgs1*Δ pairs failed to efficiently fuse (Fig. 4C,D; Bendezu and Martin 2013). While these cells were able to assemble a fusion focus, this focus was transient, often breaking up in multiple dots and showing multiple cycles of formation and disappearance (Fig. 4A,B,E; Supplemental Movie S5). Glucanases were also unfocalized in this mutant (Fig. 4H). While the molecular mechanism by which Rgs1 influences Map3 focalization remains to be established, these observations further support the model that pheromone signaling local concentration stabilizes the fusion focus, which in turn allows the precise delivery of glucanases to pierce the cell wall for fusion. Because the focus was significantly less stable in *rgs1*Δ than in *map3^{dn9}*, Rgs1 may also regulate focus stability in additional ways independent of Map3 focalization.

Pheromone signaling stabilizes the fusion focus

If spatial focalization of pheromone signaling promotes fusion by stabilizing the fusion focus, we reasoned that it might be possible to rescue the *map3^{dn9}* fusion defect by forcing the artificial recruitment of the endocytosis-defective receptor to the fusion focus. We used the tight binding between GFP and the GFP-binding protein (GBP) (Rothbauer et al. 2006, 2008) to recruit Map3^{dn9}-GFP to Myo52-GBP-mCherry at the fusion focus (Fig. 5A). Remarkably, this combination led to recruitment of Map3^{dn9}-GFP to the fusion focus, stabilization of the focus, and a sevenfold increase in successful fusion (Fig. 5B,C,F; Supplemental Movie S6). A sevenfold increase in cell lysis was also observed (Fig. 5C). As expected, this rescue of cell fusion was abrogated upon *fus1* deletion. In the presence of Myo52-GBP-mCherry, concentration of the Map3^{dn9}-GFP

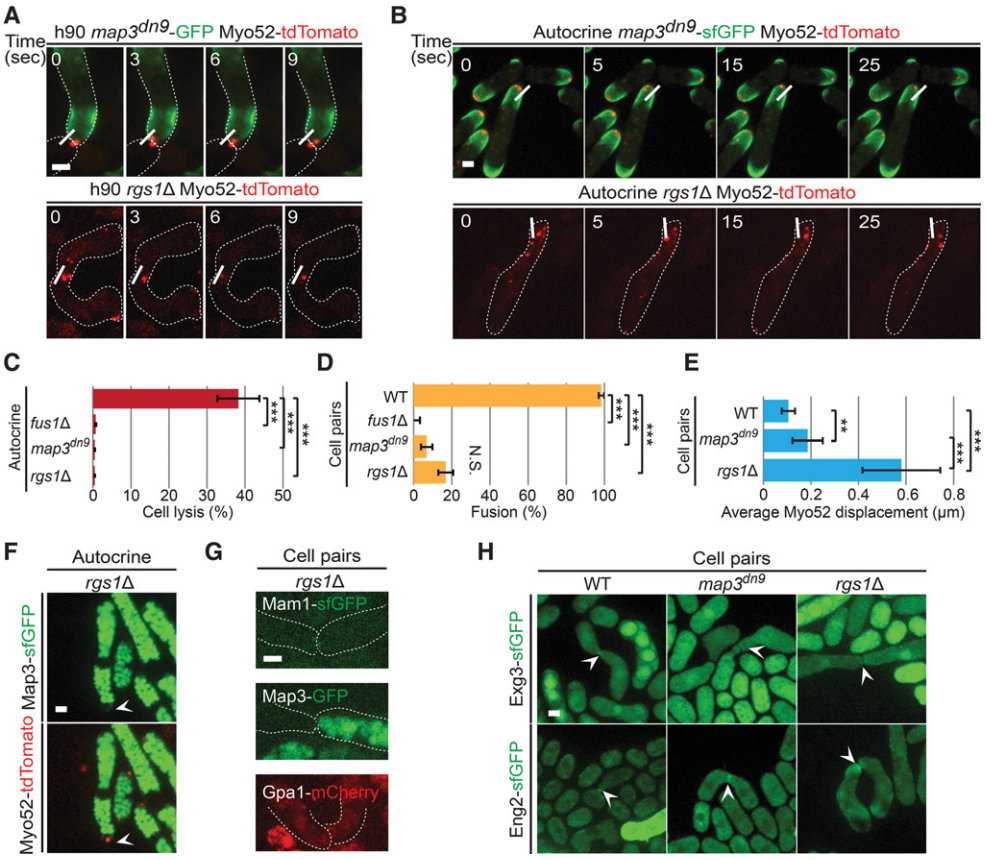

Figure 4. Loss of pheromone receptor focalization leads to severe fusion defects. (*A*) Time lapse of Myo52-tdTomato in *map3*^{dn9}*-GFP* (*top*) and *rgs1*Δ (*bottom*) mating pairs. Note the displacement of the Myo52 signal relative to the static reference line. (*Top*) Note the stable Myo52 signal in the h^- partner, which is phenotypically wild type, as it does not express *map3*^{dn9}. (*B*) Time lapse of Myo52-tdTomato in *map3*^{dn9}*-GFP* (*top*) and *rgs1*Δ (*bottom*) autocrine M cells. (*C*) Cell lysis of wild-type, *fus1*Δ, *map3*^{dn9}, and *rgs1*Δ autocrine M cells. $N > 1000$. (***) $P < 3 \times 10^{-5}$, *t*-test. (*D*) Fusion efficiency of wild-type, *fus1*Δ, *map3*^{dn9}, and *rgs1*Δ homothallic pairs. $n > 300$. (***) $P < 6 \times 10^{-4}$, *t*-test. (*E*) Mean Myo52-tdTomato displacement per 2-min time point over 30 min in homothallic wild-type and *map3*^{dn9} and *rgs1*Δ mutants. $n = 10$. (**) $P < 0.005$, *t*-test *map3*^{dn9}; (***) $P < 2 \times 10^{-5}$, *t*-test *rgs1*Δ. (*F*) In the absence of Rgs1, the Map3 pheromone receptor is unable to focalize in autocrine M cells. (*G*) Broad weak Mam1-sfGFP, Map3-GFP, and Gpa1-mCherry localization in *rgs1*Δ cell pairs. (*H*) Cell wall glucanases Exg3-sfGFP and Eng2-sfGFP focalize in wild-type but not in *map3*^{dn9} or *rgs1*Δ pairs (arrowheads). Bars, 2 μm.

signal was observed in 76% of the mating pairs (Fig. 5D), but only 43% formed a tight focus (Fig. 5E). In other cells, the Map3^{dn9}-GFP signal appeared fragmented in multiple dots, enriched over a wider zone (>0.5 μm), or not concentrated at all (Fig. 5B,E,F,H). Remarkably, we observed a very tight correlation between the appearance of Map3^{dn9}-GFP as a tight focus, the observation of a stable Myo52 focus (Fig. 5F; Supplemental Movie S7), and the ability of cells to fuse: Only cells with a tight focalization of Map3^{dn9}-GFP (but nearly all of these) fused efficiently with a partner (Fig. 5G). This observation supports the idea that the principal reason for the observed fusion defect of *map3*^{dn9} cells is the failure of the truncated receptor to accumulate at the fusion focus. Cells with a fragmented Map3^{dn9}-GFP signal frequently lysed, indicating deregulation of cell wall degradation (Fig. 5G). We conclude that tight localization of the pheromone receptor at the fusion focus is a key, necessary element to induce cell fusion.

Focalization of Byr1 MAP2K leads to fusion commitment

Pheromone signal transduction involves a dedicated MAPK cascade composed of the MAP3K Byr2, MAP2K Byr1, and MAPK Spk1. Consistent with focalization of pheromone receptors and Gpa1, Byr2, Byr1, and Spk1 were all enriched at the fusion focus of wild-type mating pairs in a Fus1-dependent manner (Fig. 6A,B). As Byr1-sfGFP exhibited the strongest signal of the three, it was used to probe MAPK cascade localization in further experiments, which revealed a perfect correlation between pheromone receptor and Byr1 focalization: Byr1 was enriched at the fusion focus in autocrine M cells, which form a fusion focus containing Map3 (Fig. 6B); it localized to the shmoo tip of M and P cells exposed to homogenous synthetic pheromones but was not focalized, consistent with the absence of a fusion focus in these cells (Supplemental Fig. S3); similarly, it was present but unfocalized at the shmoo tip of *map3*^{dn9} and

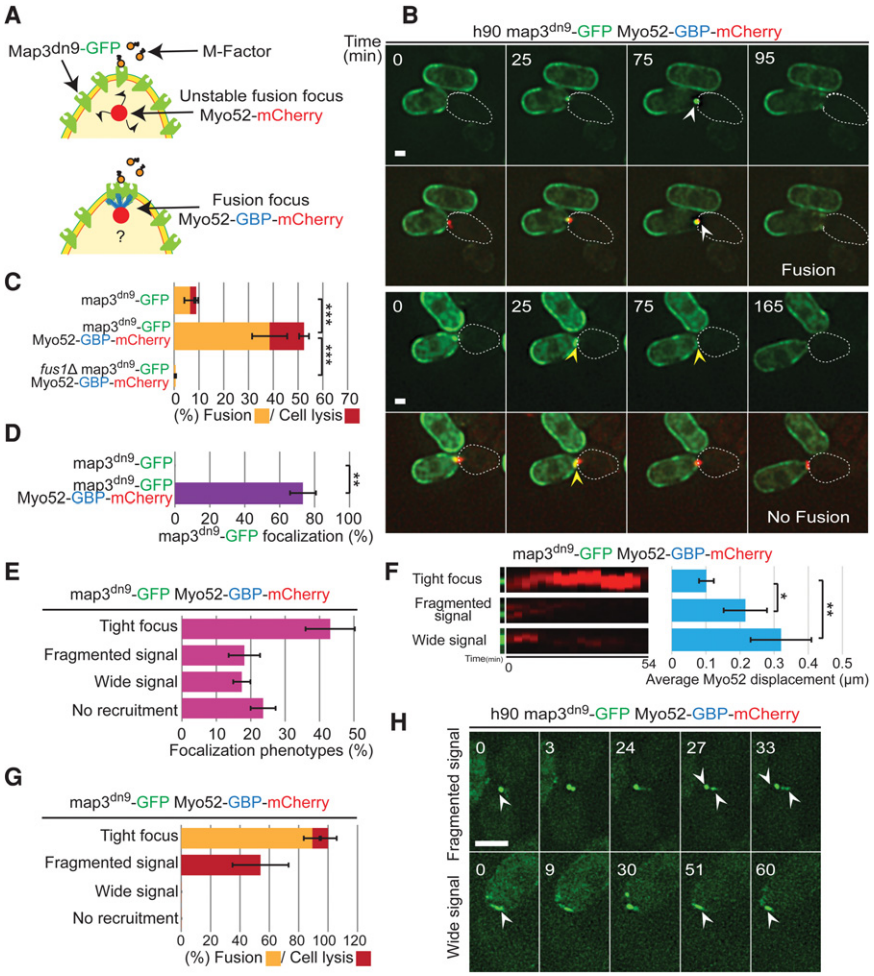

Figure 5. Forced recruitment of the pheromone receptor to the fusion focus restores cell fusion. (*A*) Scheme illustrating how the endocytosis-deficient pheromone receptor Map3^{dn9}-GFP may be concentrated at the fusion focus through Myo52-GBP-mCherry binding. (*B*) Time lapse of homothallic *h90* strains coexpressing Map3^{dn9}-GFP and Myo52-GBP-mCherry. (*Top* panels) Focalization of Map3^{dn9}-GFP (white arrowheads) correlates with fusion focus stabilization and cell fusion. (*Bottom* panels) Broader or absence of Map3^{dn9}-GFP recruitment (yellow arrowheads) correlates with motile Myo52 signal and absence of fusion. Note that the red Myo52-GBP-mCherry signal is also present in the phenotypically wild-type h^- partner cell. (*C*) Percentage of fusion and cell lysis in mating pairs of the indicated genotypes. $n > 500$. (***) $P < 5 \times 10^{-5}$, *t*-test. (*D*) Percentage of cells with focalized Map3^{dn9}-GFP. $n > 500$. (**) $P < 0.005$, *t*-test. (*E*) Percentage of cells with the indicated Map3^{dn9}-GFP distribution in homothallic *h90* strains coexpressing Map3^{dn9}-GFP and Myo52-GBP-mCherry. $n > 500$. (*F*, *left*) Kymographs of the P-cell tip in *h90 map3^{dn9}-GFP myo52-GBP-mCherry* according to Map3^{dn9}-GFP distribution as in *E*. (*Right*) Mean Myo52-GBP-mCherry displacement per 3-min time point over 48 min binned according to Map3^{dn9}-GFP distribution. $n = 5$. (*) $P < 0.02$, *t*-test fragmented signal; (**) $P < 0.007$, *t*-test wide signal. Only cells with a tight Map3^{dn9}-GFP signal display a stable focus. (*G*) Percentage of fusion and cell lysis in cells as in *E* binned according to Map3^{dn9}-GFP distribution. (*H*) Example of fragmented (*top* panels; white arrowheads) and wide (*bottom* panels; white arrowheads) Map3^{dn9}-GFP signal over time in the indicated genotype.

*rgs1*Δ mutant cells (Fig. 6C). Moreover, similar to Map3, Byr1 focalization occurred late in the fusion process, 42.5 min ± 15.5 min before fusion (Fig. 6D, compare with Fig. 3G). Interestingly, a constitutively active allele of Byr1, Byr1^{DD}, accumulated at the shmoo tip but failed to focalize, and *byr1^{DD}* mutants did not form a fusion focus and were strongly fusion-defective (Supplemental Fig. S4). Thus, focalization of Byr1 MAP2K and thus likely the whole MAPK cascade strongly correlates with fusion attempts.

To test whether MAPK focalization is the key event to induce fusion, we forced Byr1-GFP recruitment at the fusion focus in fusion-deficient strains carrying a GBP-tagged Myo52. We first generated an untagged *map3^{dn9}* allele, which was stably integrated as an extra copy in the genome. Cells carrying this allele showed phenotypes similar to, but somewhat less severe than, *map3^{dn9}-GFP* mutant cells, exhibiting a mobile fusion focus and failing to efficiently fuse (Fig. 6E and data not shown). As *map3^{dn9}* was present in addition to endogenous *map3*, this allele is dominant-negative. Remarkably, forced recruitment of Byr1-GFP to the unstable fusion focus of *map3^{dn9}* and *rgs1*Δ mutant cells led to stabilization of the fusion focus, which showed increased lifetimes in kymographs and reduced mobility by quantifying instantaneous displacement (Fig. 6 E–G; Supplemental Movies S8, S9). This led to a 2.5-fold to threefold increase in fusion/lysis compared with cells lacking Myo52-GBP-mCherry (Fig. 6E,F,H; Supplemental Movies S8, S9). Lysis was suppressed by addition of 1.2 M sorbitol or by deleting *fus1*, indicating that these cells were indeed attempting untimely fusion (Fig. 6H). Finally, even in heterothallic M cells exposed to synthetic P factor in which fusion foci are only transiently observed, the forced recruitment of Byr1-GFP to Myo52-GBP-mCherry induced the formation of a stable focus and a significant level of lysis (Fig. 6I,J). In contrast, forced recruitment of Byr1^{DD}-GFP, which never forms a fusion focus, to Myo52-GBP did not lead to formation of a fusion focus (data not shown). We conclude that recruitment of the MAP2K Byr1—and thus likely the whole pheromone–MAPK cascade at the fusion focus—is critical to consolidate the focus and promote cell fusion.

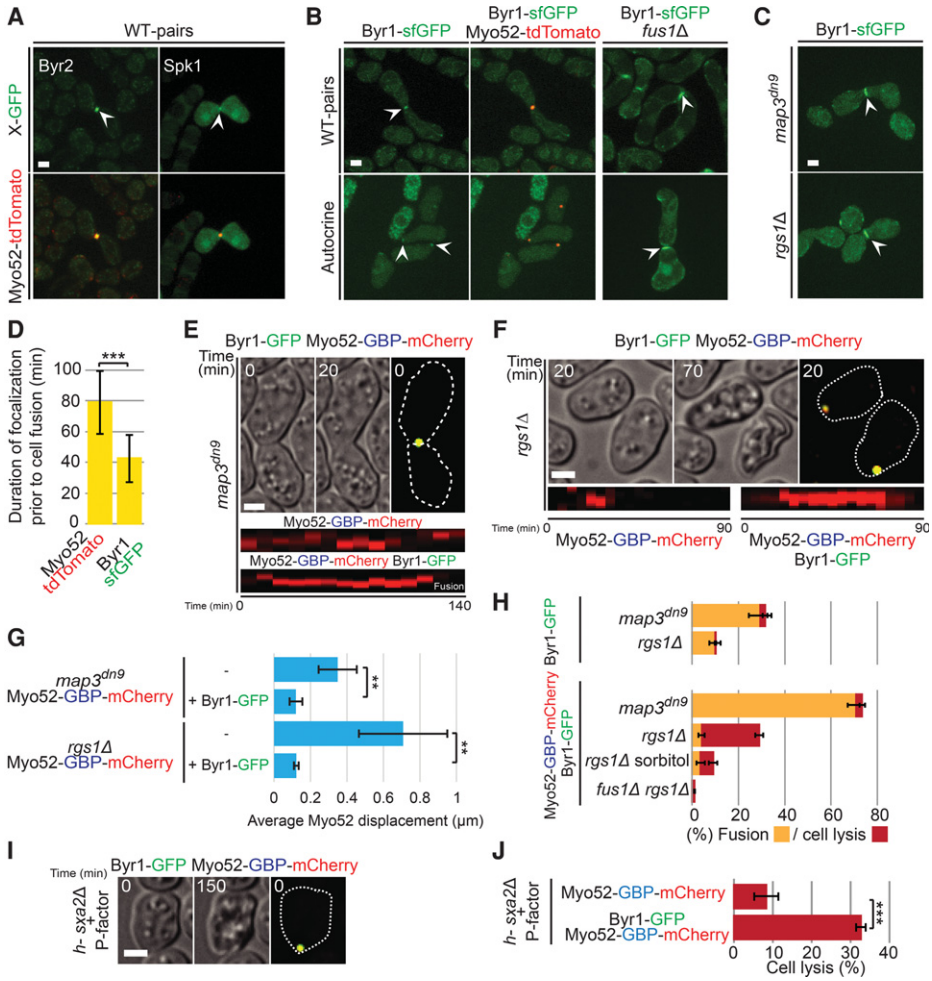

Figure 6. Focalization of MAPK cascade is critical for fusion. (*A*) Focal localization of MAP3K Byr2-GFP and MAPK Spk1-sfGFP with Myo52-tdTomato in homothallic wild-type strains. (*B*) Localization of MAP2K Byr1-sfGFP in homothallic wild-type and *fus1*Δ strains (*top*) and autocrine *fus1*$^+$ and *fus1*Δ M cells (*bottom*). (*C*) Broad localization of Byr1-sfGFP in homothallic *map3*^{dn9} and *rgs1*Δ *strains*. (*D*) Time before fusion in which Myo52-tdTomato and Byr1-sfGFP signals are focalized. $n = 20$. (***) $P < 2 \times 10^{-13}$, *t*-test. (*E*,*F*) Imaging of homothallic *h90 map3*^{dn9} (*E*) and *rgs1*Δ (*F*) strains coexpressing Byr1-GFP and Myo52-GBP-mCherry. Time is expressed in minutes. The second DIC image shows cell fusion and lysis, respectively. (*E*,*F*, *bottom*) The kymographs of the cell tip show an unstable or transient focus of Myo52-GBP-mCherry in *map3*^{dn9} and *rgs1*Δ, respectively, and stabilization upon Byr1-GFP recruitment. (*G*) Mean Myo52-GBP-mCherry displacement per 10-min time point over 130 min in homothallic *map3*^{dn9} and *rgs1*Δ mutants expressing or not expressing Byr1-GFP. $n = 5$. (**) $P < 0.01$, *t*-test *map3*^{dn9}; (**) $P < 0.009$, *t*-test *rgs1*Δ. (*H*) Percentage of cell fusion and lysis of homothallic *h90 map3*^{dn9} and *rgs1*Δ strains expressing Byr1-GFP or coexpressing Byr1-GFP and Myo52-GBP-mCherry. $n > 500$ for three independent experiments. (*I*) Heterothallic *h*$^-$ *sxa2*Δ cells treated with 10 μg/mL synthetic P factor coexpressing Byr1-GFP and Myo52-GBP-mCherry. Time is in minutes. (*J*) Percentage of cell lysis of heterothallic *h*$^-$ *sxa2*Δ cells expressing Myo52-GBP-mCherry or coexpressing Byr1-GFP and Myo52-GBP-mCherry 14 h after 10 μg/mL synthetic P-factor addition. $n > 500$ for three independent experiments. (***) $P < 2 \times 10^{-4}$, *t*-test. Bars, 2 μm.

Discussion

Here, we addressed how cells make the decision to fuse. While this decision is expected to be coupled with the formation of a cell pair, we established that it requires neither cell–cell contact nor a signal distinct from that inducing previous events. Instead, it relies on diffusible pheromones, which also signal the earlier stages of cell differentiation and cell polarization. Importantly, we showed that the fusion information is coded in their spatially focalized distribution. This focalized organization results from a positive feedback loop between pheromone signaling and the actin fusion focus, which underlies the local concentration of pheromone release and signal activation, leading to the concentration at the fusion site of the MAPK cascade. In turn, this local concentration of the MAPK module drives fusion commitment by stabilizing the actin focus.

How does focalization of pheromone signaling happen?

The autocrine M cells show that the coexpression of a pheromone receptor and its ligand in the same cell is sufficient to drive the formation of a single focus, indicative

of a positive feedback motif (Fig. 7). We propose that this positive feedback relies on two key elements: (1) the signaling machinery, which includes the M-factor receptor Map3, its ligand transported by the Mam1 transporter, and the MAPK cascade, and (2) the actin fusion focus, consisting principally of the formin Fus1 and type V myosins.

Two main reactions underlie this positive feedback. One reaction involves Fus1 promoting the assembly of actin cables along which Map3 and Mam1, both transmembrane proteins, are delivered to the plasma membrane in exocytic vesicles. At the plasma membrane, endocytosis retrieves Map3 (Hirota et al. 2001), thus opposing lateral diffusion and ensuring Map3 enrichment at the site of delivery. The Mam1 transporter is likely also retrieved through endocytosis, as has been demonstrated for its budding yeast homolog, Ste6 (Kolling and Hollenberg 1994). This leads to the activation of Map3 with maximal ligand concentration at or close to sites of exocytic delivery and consequent recruitment of the MAPK module at these sites. It is noteworthy that spatial restriction of both ligand and receptor is required, indicating that local graded pheromone distribution rather than its absolute concentration significantly contributes to focalization of the downstream signal. This also suggests that cells may have the ability to measure the steepness of the pheromone profile. The second reaction consists of the focalization of the MAPK module promoting the stabilization of the actin fusion focus. The molecular details of this reaction remain to be defined. It may be conceptually similar to how G-protein and MAPK polarization constrain the polarity patch for gradient tracking by forming a positive feedback on Cdc42 GTPase activation (Hegemann et al. 2015; McClure et al. 2015). Alternatively, the MAPK signal may act more directly on Fus1 activation or recruitment or involve other elements of the fusion focus. In the autocrine situation, the positive feedback motif created by these two reactions underlies a symmetry-breaking event leading to the formation of a single constrained actin focus, which sharpens the localization of the signaling machinery, which in turn further constrains the focus.

In the natural situation involving the pairing of cells of distinct mating types, the only likely difference is that the pheromone ligand for receptor activation is delivered by the partner cell (Fig. 7). In this case, the site of pheromone release from one cell defines the site of receptor activation and thus actin fusion focus stabilization in the second cell, which in turn promotes the local release of pheromone to sharpen the site of signaling in the first one. Thus, the feedback system is established upon bilateral cell pairing, ensuring that the cells do not focalize their signaling machinery in the absence of a mating partner.

In summary, at its core, pheromone signaling focalization relies on a positive feedback loop, similar to other symmetry-breaking systems (Motegi and Seydoux 2013; Yi et al. 2013; Martin 2015) in which Fus1 promotes the delivery of the receptor and its activator, and the activated receptor promotes Fus1 function.

Spatial focalization of MAPK signaling as a cellular decision

One notable and perhaps unexpected result is that forced recruitment of either pheromone receptor or the downstream MAP2K to the fusion focus induces fusion attempts. Because both pheromone receptor and Byr1 MAP2K recruitments have the same phenotypic consequence of stabilizing the fusion focus, it is unlikely that this is caused simply by tethering the fusion focus to the endocytosis-deficient receptor at the plasma membrane or forcing a kinase–substrate contact. Rather, in conjunction with the observation that pheromone signaling focalization coincides with the commitment of wild-type mating pairs to fusion, this result suggests that the cellular decision to fuse is triggered by the spatial concentration of MAPK signaling.

Mechanisms that underlie cellular decisions must typically convert a graded signal (here pheromones) into an all-or-none response (here the decision to fuse). Classical work on the MAPK cascade has shown that it can function as a switch that converts a low-level signal into a maximal

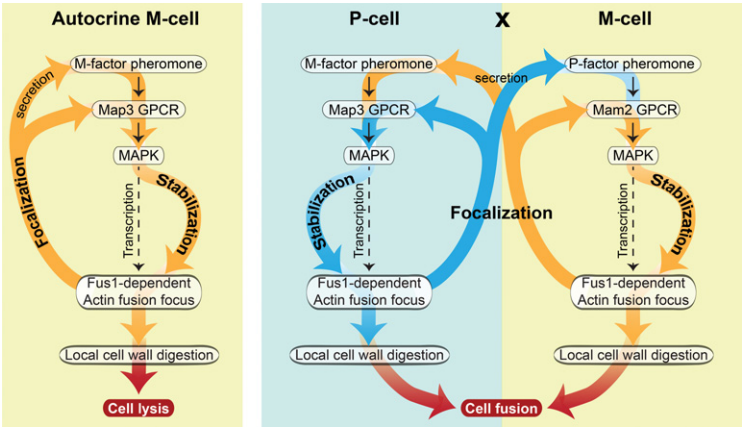

Figure 7. A positive feedback between the signaling machinery and the actin fusion focus drives commitment to cell–cell fusion. Thin black arrows show the pheromone signaling cascade. Thick colored arrows highlight the spatial regulation that forms the basis of the positive feedback underlying the cellular decision to fuse. Initiation of the Fus1-dependent actin fusion focus upon transcriptional activation of Fus1 spatially restricts the secretion of the pheromone ligands as well as the surface delivery of its receptors. This leads to local recruitment of the MAPK cascade. This local MAPK enrichment in turn restricts the mobility of the fusion focus, thus forming a positive feedback motif that leads to strong focalization of the pheromone/MAPK signal and stabilization of the fusion focus. This spatial stabilization is critical to promote local cell wall digestion by enrichment of cell wall hydrolases at a static position. (*Left*) In an autocrine system, the pheromone ligand and its receptor drive this positive feedback within a single cell, leading to cell lysis upon cell wall digestion. (*Right*) In the natural situation of two mating partners, local pheromone release from one cell feeds into focalization in the other cell, thus coupling the positive feedback to the presence and position of the partner cell to achieve cell fusion.

signal (Ferrell 1996). However, the MAPK module is highly versatile and can be modulated in various cell types and situations to generate distinct graded or switch-like outputs (Inder et al. 2008; English et al. 2015). For instance, the MAPK pheromone pathway in *S. cerevisiae* exhibits an essentially graded response to induce gene expression proportional to pheromone concentration (Poritz et al. 2001; Paliwal et al. 2007), but its role in inducing the formation of the mating projection is switch-like, a behavior dependent on the MAPK scaffold Ste5 (Hao et al. 2008; Malleshaiah et al. 2010). The *S. pombe* pheromone MAPK module, like the mammalian Raf–MEK–ERK cascade, which can functionally replace it (Hughes et al. 1993), lacks a scaffold protein. Interestingly, synthetic biological approaches have shown that a simple concentration increase of sequential Raf–MEK–ERK kinases is sufficient to lower the activation threshold and enhance ultrasensitivity, leading to full activation (O'Shaughnessy et al. 2011). This evidence leads us to propose that the local concentration of the pheromone MAPK cascade at the fusion site in *S. pombe* represents a natural situation in which the cell exploits the ultrasensitivity of the MAPK cascade to convert it to the fully active state, which, due to the spatially restricted location in which this takes place, drives an essentially irreversible decision to fuse.

Similar spatial rearrangements may control cellular decisions in other cell types. The spatial organization of signaling molecules is generally thought to be important for signal transduction (Kiel and Serrano 2012). For instance, during adaptive immunity, activation of the T-cell receptor is thought to result from its spatial segregation from bulky inactivating phosphatases that are sterically excluded from the zone of receptor engagement with the antigen-presenting cell (Davis and van der Merwe 2006; James and Vale 2012). Similarly, distinct subcellular localization of GPCR-mediated signaling and the MAPK cascade can drive distinct cellular responses in various cell types (Harding et al. 2005; Inder et al. 2008; West and Hanyaloglu 2015), although it is not known to what extent spatial changes are harnessed to modulate the signal. It will be interesting to probe whether other cells spatially reorganize their signaling pathways to change the system's output.

Mechanistic function of fusion focus stabilization

How does spatial stabilization of the fusion focus promote cell fusion? One critical role of the fusion focus is to promote the local delivery of glucanases that catalyze the hydrolysis of the bonds in glucan polymers to locally dissolve the cell wall, whereas glucan synthases are more broadly distributed (Dudin et al. 2015). In the absence of the fusion focus, in *fus1*Δ pairs, both enzymatic activities occupy similarly broad distributions, leading to cell wall remodeling for polarized growth but not cell wall dissolution (Dudin et al. 2015). Glucanases are likely also broadly distributed in $byr1^{DD}$ mutants, in which focalization fails. Similarly, in $map3^{dn9}$ or *rgs1*Δ mutant pairs that display an unstable fusion focus, no sharp glucanase localization can be detected. We hypothesize that glucanases are still locally released at the fusion focus, but their (broad or nearly undetectable) localization reflects the time-averaged consequence of secretion from a motile site, which is similar to the localization resulting from secretion over a broad region. Thus, in the absence of fusion focus stabilization, the cell wall cannot be pierced, and cells instead continue to grow. In contrast, immobilization of the fusion focus leads to local imbalance in favor of hydrolytic activity such that the cell wall is pierced for fusion.

Timing of the decision to fuse

Because yeast cell growth is driven by turgor pressure, the cell wall is essential to preserve cell integrity. Therefore, the decision to stabilize the fusion focus to locally digest the cell wall has to be precisely coordinated with the formation of cell pairs. Indeed, untimely fusion focus stabilization in autocrine cells or upon forced signaling focalization leads to cell lysis because cell wall digestion occurs in the absence of an attached partner cell. Interestingly, ~60% of autocrine M cells do not lyse, at least within the time frame of our experiments, whereas wild-type mating pairs almost always fuse. Thus, while focalization of pheromone signaling serves as a fusion signal, the zone of cell–cell contact may offer a favorable context for this signal, for instance, by constraining diffusion in the cell wall to two dimensions, thus promoting a local increase in pheromone levels, as proposed previously for cell wall remodeling enzymes (Huberman and Murray 2014). Alternatively, cells may possess built-in break mechanisms that antagonize the positive feedback for focalization, which are alleviated upon cell–cell contact. Future work should establish how the decision to fuse is taken at the appropriate time.

Materials and methods

Strains, media, and growth conditions

Strains used in this study are listed in Supplemental Table S1. For assessing cells during exponential growth, cells were grown in rich medium (YE), Edinburgh minimal medium (EMM), or minimal sporulation medium with nitrogen (MSL + N) supplemented with amino acids as required. For assessing cells during the mating process, liquid or agar minimal sporulation medium without nitrogen (MSL – N) was used (Egel et al. 1994; Vjestica et al. 2016). All live-cell imaging was performed on MSL – N agarose pads (Vjestica et al. 2016) or in microfluidics chambers (described below). Mating assays were performed as in Vjestica et al. (2016).

Gene tagging was performed at endogenous genomic loci at the 3′ end, yielding C-terminally tagged proteins as described (Bähler et al. 1998) and was confirmed by diagnostic PCR for both sides of the gene insertion. Tagging with sfGFP was performed as in Dudin et al. (2015). The map3-GFP tag was obtained from Hirota et al. (2001). We also generated a map3-sfGFP, in which sfGFP was inserted at the 3′ end of the *map3* ORF and likely disrupted the nested gene in the opposite direction without obvious ill effects. This strain was used only in Supplemental Figure S3, for which the result was also confirmed with a *map3-GFP* strain. Tagging with GBP-mCherry was performed at the C termini of endogenous genomic loci.

Construction of plasmid for GBP-mCherry tagging was done as follows. First, a GBP-mCherry fragment was amplified from

pSO216 (a gift from Dr. Snezhana Oliferenko, King's College, London) using primers osm3329 (5′-TCCTTAATTAACATGG CCGATGTGCAGCTGGTGG-3′) and osm3331 (5′-CCCGGCG CGCC**TTA**CTTGTACAGCTCGTCCATGC-3′), digested with PacI and AscI, and ligated to similarly treated *pFA6-kanMX* (pSM644) to generate *pFA6-GBP-mcherry-kanMX* (pAV237; a kind gift from Dr. Aleksandar Vjestica, University of Lausanne). Second, a *bleMX* cassette for zeocine resistance was excised from the *pFA6-bleMX* (pSM694) plasmid by digestion with AscI and SacII and ligated to similarly treated pAV237 to generate *pFA6-GBP-mcherry-bleMX* (pSM1768). In primer sequences, restriction sites are underlined, and the stop codon is in bold.

For the construction of M-cell autocrine strains, a pFA6a-map3 plasmid was used as a template. *map3* was amplified from a wild-type P cell using primers osm2501 (5′-ACTcggatcccATG TTGCCTATTGGGATTTTCTATC-3) and osm2502 (5′-GGA agatctGCACAAAACTGGCTACAAGAAGGTG-3), digested with BamHI and BglII, and ligated to similarly treated pFA6a-hphMX6 (pSM693) (Hentges et al. 2005), producing pFA6a-Map3-hphMX6 (pSM1521). We then used this vector as a template for PCR-based amplification and targeted replacement of *mam2* in parental M-cell strains using primers osm2503 (5′-TGCTTTACAAA TCACATTTTTAAACTTCTTAAACTAAAAAAATCTCGGGT TTATATTGTTCTTGCTCCCTCTGACATTATGTTGCCTAT TGGGATTTTCTATC-3) and osm2504 (5′-AAAAAACCGTCTA TGTTATTTGGGACTGTTATTGAGCCAGTATTAGGAATTA TCAAAAAAGATACATTCAGGCGTAAGGAATTCGAGCTC GTTTAAAC-3).

To generate *map3^{dn9}-sfGFP* autocrine M cells, we truncated the last 228 nucleotides of the *map3*-coding region in the M-cell autocrine cells obtained above by integration of sfGFP, yielding a Map3^{dn9}-sfGFP allele truncated at amino acid 290, as described in Hirota et al. (2001). sfGFP was amplified from pFA6a-sfGFP-kanMX6 (pSM1538) using osm3789 (5′-AAGGTTGCAT TAATCCTTTGGTCTCTTTTGGTATGGCTTCCTTTTACCA AAAATACCGCGTTGGGTCGTCATGCACAACGGATCCCC GGGTTAATTAA-3′) and osm1453 (5′-GATAGAACGTTTGAT ATCAAACATACTCCCAGTGACGATTATTCGATTTCTGAT GAATCTGAAACTAAAAAGTGGACGCGGATCCCCGGGTT AATTAA-3′).

Construction of a strain expressing the untagged *map3^{dn9}* allele was done by integrating *map3^{dn9}* under the *map3* promoter at the *ura4$^+$* locus. First, a fragment encompassing the *map3* promoter and *map3^{dn9}*-coding regions was amplified from genomic DNA of FB404 with primers osm4083 (5′-ccgctcgagACGCGT AAATGTGTACGCG-3′) and osm4084 (5′-tcccccgggg**tta**TTGT GCATGACGACCCAACG-3′), digested with XhoI and XmaI, and ligated to similarly treated *pJK211-ura4-3′ UTR-AfeI-ura4-5′ UTR*, a single integration vector (kind gift from Aleksandar Vjestica), to generate plasmid pSM1921 (*pJK211-ura4-3′ UTR-AfeI-ura4-5′ UTR-p^{map3}-map3^{dn9}*). Second, the *nmt1* terminator was excised from pSM1449 by digestion with XmaI and NotI and ligated in similarly treated pSM1921 to generate plasmid pSM1935 (*pJK211-ura4-3′ UTR-AfeI-ura4-5′ UTR-p^{map3}-map3^{dn9}-t^{nmt1}*). pSM1935 digested with AfeI was stably integrated as a single copy at the *ura4$^+$* locus in the yeast genome. In primer sequences, restriction sites are underlined, and the stop codon is in bold.

Construction of strains expressing the constitutively active *byr1^{DD}* allele was done by integration of *byr1^{DD}* at the endogenous *byr1* locus. The Byr1^{DD} mutant has the two following point mutations, S214D and T218D, as described previously (Ozoe et al. 2002). First, a fragment including the byr1-coding region and 5′ and 3′ extensions was amplified from genomic DNA with primers osm1837 (5′-tccccgggGATCTAATAATGCTTTG TATTAAG-3′) and osm1838 (5′-aaaactgcagTTGGCTTATACG TAATTGCCAAG-3′), digested with PstI and XmaI, and ligated to similarly treated pSM1232 to generate plasmid pSM1668 (pSP72-*byr1*). Second, pSM1668 was subjected to site-directed mutagenesis with primers osm1860 (5′-GGTGAACTAGTTAA C**GAC**GTTGCTCAAACGTTTG-3′) and osm1861 (5′-CAAAC GTTTGAGCAAC**GTC**GTTAACTAGTTCACC-3′) to generate plasmid pSM1677 (pSP72-*byr1-S214D*). Third, pSM1677 was subjected to site-directed mutagenesis with primers osm1862 (5′-GT TAACGACGTTGCTCAA**GAC**TTTGTGGGGACTTCAAC-3′) and osm1863 (5′-GTTGAAGTCCCCACAAA**GTC**TTGAGCAA CGTCGTTAAC-3′) to generate plasmid pSM1687 (pSP72-*byr1-S214DT218D*). Finally, pSM1687 digested with PstI and XmaI was stably integrated as a single copy at the *byr1* locus in the yeast genome. In primer sequences, restriction sites are underlined, and inserted mutations are in bold.

Mating assays

Mating assays, including treatment of autocrine M cells, were performed as in Bendezu and Martin (2013), Dudin et al. (2015), and Vjestica et al. (2016). Briefly, precultures of cells were grown at 25°C to OD600 = 0.4–1 in MSL + N. Cultures were then diluted to OD600 = 0.025 in MSL + N (for heterothallic crosses, cells were mixed in equal parts) and grown for 18–20 h to OD600 = 0.4 – 1 at 25°C in MSL + N. Cells were harvested by centrifugation, washed three times with MSL – N, and, unless indicated otherwise, mounted onto MSL – N 2% agarose pads that were incubated for either 1 h at 25°C before imaging in overnight movies or overnight at 18°C before imaging. Fusion efficiency was measured as in Dudin et al. (2015). The percentage of lysis was calculated as percentage lysis = number of lysing cells/total amount of shmooing cells × 100. For mating assays in microfluidic chambers, mating cells were prepared as described above but were not mounted on agarose pads. Instead, cells were loaded into a microfluidic cell culture chamber (CellASIC Corp., Y04C) with the ONIX (CellASIC Corp.) as an automated controller, allowing rapid medium flow. Cells in MSL – N were loaded into the microfluidic chamber and left for 2 h at 25°C in the absence of fluid flow. To transiently perturb any diffusible gradient, fresh MSL – N medium was flowed at a rate of 13 µL/h (5 psi) for 10 min. To obtain control cells without flow, scotch tape was tightly fixed on the first six air channels of the manifold of the corresponding chamber. For pheromone treatments, P-factor pheromone was purchased from Pepnome and used from a stock solution of 1 mg/mL in methanol. M factor was synthetized and purchased from Schafer-N and used from a stock solution of 2 mg/mL in methanol. Different concentrations of pheromones were directly added to the agarose pads. Cells were then incubated overnight at 25°C prior to imaging. Methanol was used as a control.

Experiments on autocrine M cells were performed similarly to normal homothallic strains. However, as the autocrine cells are extremely sensitive to the absence of nitrogen, cells were usually maintained in MSL + N at an OD = 600 < 0.6. Autocrine cells were washed with MSL – N and placed directly on MSL – N agarose pads. For experiments including external pheromones, M factor was added directly in the agarose pads, and cells were incubated for 16 h.

Microscopy and image analysis

The DeltaVision platform (Applied Precision) described previously (Bendezu and Martin 2013) was used mainly for time-lapse imaging overnight or during microfluidic experiments (Figs. 1, 2D,E, 3A,B,D–F, 4F–H, 6B–J; Supplemental Figs. S1, S2A–C). To limit photobleaching, overnight movies were captured by OAI (optical axis integration) imaging of a 4.6-µm *z* section, which is

essentially a real time *z* sweep (Figs. 2D, 3A,F, 4F, 6B,F). Spinning-disk microscopy, also described previously (Bendezu and Martin 2013), was used mainly for quantitative analyses of fusion efficiency, cell lysis, cell size, and calcofluor staining as well as high temporal resolution and *Z*-stack maximal projection images (Figs. 2B,C,E, 3C–E, 4A–E, 5A–H, 6A,B; Supplemental Figs. S2A–C,E, S3, S4). To measure the mobility of the fusion focus (Figs. 1E, 5D), the *X* and *Y* coordinates of the highest-intensity pixel of the Myo52-tdTomato signal were used to measure the instantaneous displacement between each time point (every 2 min) in each mating partner. When Myo52 signal was broad, we recorded the coordinates of the maximum fluorescence intensity. Displacement was calculated as $\sqrt{[(X_n\text{-}X_{n-1})^2+(Y_n\text{-}Y_{n-1})^2]}$. This measure was then averaged over the length of the time-lapse acquisition. Kymographs in Figures 5 and 6 were constructed in ImageJ version 1.47 (National Institutes of Health) by drawing a 3-pixel-wide line at the cell tip.

Gene expression quantifications

Fluorescence intensities of Mam1-sfGFP, Fus1-sfGFP, and Map3-sfGFP in Figure 2B were measured in ImageJ using a manually drawn line around the entire cells in sum projections of seven slices over 4-µm total depth. Background fluorescence for sfGFP was measured from similarly treated cells lacking sfGFP and was subtracted from the original measurements.

Figures were assembled with Adobe Photoshop CS5 and Adobe Illustrator CS5. All error bars are standard deviations. All experiments were done a minimum of three independent times, and statistical analysis was done across repeats of the same experiment.

Acknowledgments

We thank S. Oliferenko, A. Vjestica, M. Yamamoto, and the Yeast Genetic Resource Center Japan for reagents, and R. Benton, S. Pelet, J. van der Meer, and members of the Martin laboratory for critical reading of the manuscript. This work was supported by funding from the Swiss National Science Foundation (grant 31003A_155944). O.D., L.M., and S.G.M. conceived the studies and set up the methodology. O.D. and L.M. performed the investigations (O.D. worked on the microfluidics, the autocrine system, and the synthetic pheromone treatments, and L.M. worked on the synthetic pheromone treatments and reconstitution of focalization). S.G.M. wrote the original draft, and O.D., L.M., and S.G.M. wrote, reviewed, and edited the manuscript. S.G.M. acquired funding.

References

Abmayr SM, Pavlath GK. 2012. Myoblast fusion: lessons from flies and mice. *Development* **139:** 641–656.

Aguilar PS, Baylies MK, Fleissner A, Helming L, Inoue N, Podbilewicz B, Wang H, Wong M. 2013. Genetic basis of cell–cell fusion mechanisms. *Trends Genet* **29:** 427–437.

Ayscough KR, Drubin DG. 1998. A role for the yeast actin cytoskeleton in pheromone receptor clustering and signalling. *Curr Biol* **8:** 927–930.

Bähler J, Wu JQ, Longtine MS, Shah NG, McKenzie A III, Steever AB, Wach A, Philippsen P, Pringle JR. 1998. Heterologous modules for efficient and versatile PCR-based gene targeting in *Schizosaccharomyces pombe*. *Yeast* **14:** 943–951.

Bendezu FO, Martin SG. 2013. Cdc42 explores the cell periphery for mate selection in fission yeast. *Curr Biol* **23:** 42–47.

Brizzio V, Gammie AE, Nijbroek G, Michaelis S, Rose MD. 1996. Cell fusion during yeast mating requires high levels of a-factor mating pheromone. *J Cell Biol* **135:** 1727–1739.

Christensen PU, Davey J, Nielsen O. 1997. The *Schizosaccharomyces pombe* mam1 gene encodes an ABC transporter mediating secretion of M-factor. *Mol Gen Genet* **255:** 226–236.

Croft W, Hill C, McCann E, Bond M, Esparza-Franco M, Bennett J, Rand D, Davey J, Ladds G. 2013. A physiologically required G protein-coupled receptor (GPCR)–regulator of G protein signaling (RGS) interaction that compartmentalizes RGS activity. *J Biol Chem* **288:** 27327–27342.

Davey J. 1992. Mating pheromones of the fission yeast *Schizosaccharomyces pombe*: purification and structural characterization of M-factor and isolation and analysis of two genes encoding the pheromone. *EMBO J* **11:** 951–960.

Davey J, Nielsen O. 1994. Mutations in cyr1 and pat1 reveal pheromone-induced G1 arrest in the fission yeast *Schizosaccharomyces pombe*. *Curr Genet* **26:** 105–112.

Davis SJ, van der Merwe PA. 2006. The kinetic-segregation model: TCR triggering and beyond. *Nat Immunol* **7:** 803–809.

Doyle A, Martin-Garcia R, Coulton AT, Bagley S, Mulvihill DP. 2009. Fission yeast Myo51 is a meiotic spindle pole body component with discrete roles during cell fusion and spore formation. *J Cell Sci* **122:** 4330–4340.

Dudin O, Bendezu FO, Groux R, Laroche T, Seitz A, Martin SG. 2015. A formin-nucleated actin aster concentrates cell wall hydrolases for cell fusion in fission yeast. *J Cell Biol* **208:** 897–911.

Egel R, Willer M, Kjaerulff S, Davey J, Nielsen O. 1994. Assessment of pheromone production and response in fission yeast by a halo test of induced sporulation. *Yeast* **10:** 1347–1354.

Ene IV, Bennett RJ. 2014. The cryptic sexual strategies of human fungal pathogens. *Nat Rev Microbiol* **12:** 239–251.

English JG, Shellhammer JP, Malahe M, McCarter PC, Elston TC, Dohlman HG. 2015. MAPK feedback encodes a switch and timer for tunable stress adaptation in yeast. *Sci Signal* **8:** ra5.

Ferrell JE Jr. 1996. Tripping the switch fantastic: how a protein kinase cascade can convert graded inputs into switch-like outputs. *Trends Biochem Sci* **21:** 460–466.

Hao N, Nayak S, Behar M, Shanks RH, Nagiec MJ, Errede B, Hasty J, Elston TC, Dohlman HG. 2008. Regulation of cell signaling dynamics by the protein kinase-scaffold Ste5. *Mol Cell* **30:** 649–656.

Harding A, Tian T, Westbury E, Frische E, Hancock JF. 2005. Subcellular localization determines MAP kinase signal output. *Curr Biol* **15:** 869–873.

Hegemann B, Unger M, Lee SS, Stoffel-Studer I, van den Heuvel J, Pelet S, Koeppl H, Peter M. 2015. A cellular system for spatial signal decoding in chemical gradients. *Dev Cell* **35:** 458–470.

Hentges P, Van Driessche B, Tafforeau L, Vandenhaute J, Carr AM. 2005. Three novel antibiotic marker cassettes for gene disruption and marker switching in *Schizosaccharomyces pombe*. *Yeast* **22:** 1013–1019.

Hirota K, Tanaka K, Watanabe Y, Yamamoto M. 2001. Functional analysis of the C-terminal cytoplasmic region of the M-factor receptor in fission yeast. *Genes Cells* **6:** 201–214.

Huberman LB, Murray AW. 2014. A model for cell wall dissolution in mating yeast cells: polarized secretion and restricted diffusion of cell wall remodeling enzymes induces local dissolution. *PLoS One* **9:** e109780.

Hughes DA, Ashworth A, Marshall CJ. 1993. Complementation of byr1 in fission yeast by mammalian MAP kinase kinase requires coexpression of Raf kinase. *Nature* **364:** 349–352.

Imai Y, Yamamoto M. 1994. The fission yeast mating pheromone P-factor: its molecular structure, gene structure, and ability to

induce gene expression and G1 arrest in the mating partner. *Genes Dev* **8:** 328–338.
Inder K, Harding A, Plowman SJ, Philips MR, Parton RG, Hancock JF. 2008. Activation of the MAPK module from different spatial locations generates distinct system outputs. *Mol Biol Cell* **19:** 4776–4784.
James JR, Vale RD. 2012. Biophysical mechanism of T-cell receptor triggering in a reconstituted system. *Nature* **487:** 64–69.
Kiel C, Serrano L. 2012. Challenges ahead in signal transduction: MAPK as an example. *Curr Opin Biotechnol* **23:** 305–314.
Kitamura K, Shimoda C. 1991. The *Schizosaccharomyces pombe* mam2 gene encodes a putative pheromone receptor which has a significant homology with the *Saccharomyces cerevisiae* Ste2 protein. *EMBO J* **10:** 3743–3751.
Kjaerulff S, Davey J, Nielsen O. 1994. Analysis of the structural genes encoding M-factor in the fission yeast *Schizosaccharomyces pombe*: identification of a third gene, mfm3. *Mol Cell Biol* **14:** 3895–3905.
Kolling R, Hollenberg CP. 1994. The ABC-transporter Ste6 accumulates in the plasma membrane in a ubiquitinated form in endocytosis mutants. *EMBO J* **13:** 3261–3271.
Lluis F, Cosma MP. 2010. Cell-fusion-mediated somatic-cell reprogramming: a mechanism for tissue regeneration. *J Cell Physiol* **223:** 6–13.
Lu X, Kang Y. 2009. Cell fusion as a hidden force in tumor progression. *Cancer Res* **69:** 8536–8539.
Malleshaiah MK, Shahrezaei V, Swain PS, Michnick SW. 2010. The scaffold protein Ste5 directly controls a switch-like mating decision in yeast. *Nature* **465:** 101–105.
Martin SG. 2015. Spontaneous cell polarization: feedback control of Cdc42 GTPase breaks cellular symmetry. *Bioessays* **37:** 1193–1201.
McClure AW, Minakova M, Dyer JM, Zyla TR, Elston TC, Lew DJ. 2015. Role of polarized G protein signaling in tracking pheromone gradients. *Dev Cell* **35:** 471–482.
Merlini L, Dudin O, Martin SG. 2013. Mate and fuse: how yeast cells do it. *Open Biol* **3:** 130008.
Merlini L, Khalili B, Bendezu FO, Hurwitz D, Vincenzetti V, Vavylonis D, Martin SG. 2016. Local pheromone release from dynamic polarity sites underlies cell–cell pairing during yeast mating. *Curr Biol* **26:** 1117–1125.
Michaelis S, Herskowitz I. 1988. The a-factor pheromone of *Saccharomyces cerevisiae* is essential for mating. *Mol Cell Biol* **8:** 1309–1318.
Minc N, Boudaoud A, Chang F. 2009. Mechanical forces of fission yeast growth. *Curr Biol* **19:** 1096–1101.
Morrow CA, Fraser JA. 2009. Sexual reproduction and dimorphism in the pathogenic basidiomycetes. *FEMS Yeast Res* **9:** 161–177.
Motegi F, Seydoux G. 2013. The PAR network: redundancy and robustness in a symmetry-breaking system. *Philos Trans R Soc Lond B Biol Sci* **368:** 20130010.
Neiman AM, Stevenson BJ, Xu HP, Sprague GF Jr, Herskowitz I, Wigler M, Marcus S. 1993. Functional homology of protein kinases required for sexual differentiation in *Schizosaccharomyces pombe* and *Saccharomyces cerevisiae* suggests a conserved signal transduction module in eukaryotic organisms. *Mol Biol Cell* **4:** 107–120.
Obara T, Nakafuku M, Yamamoto M, Kaziro Y. 1991. Isolation and characterization of a gene encoding a G-protein α subunit from *Schizosaccharomyces pombe*: involvement in mating and sporulation pathways. *Proc Natl Acad Sci* **88:** 5877–5881.
O'Shaughnessy EC, Palani S, Collins JJ, Sarkar CA. 2011. Tunable signal processing in synthetic MAP kinase cascades. *Cell* **144:** 119–131.
Ozoe F, Kurokawa R, Kobayashi Y, Jeong HT, Tanaka K, Sen K, Nakagawa T, Matsuda H, Kawamukai M. 2002. The 14–3–3 proteins Rad24 and Rad25 negatively regulate Byr2 by affecting its localization in *Schizosaccharomyces pombe*. *Mol Cell Biol* **22:** 7105–7119.
Paliwal S, Iglesias PA, Campbell K, Hilioti Z, Groisman A, Levchenko A. 2007. MAPK-mediated bimodal gene expression and adaptive gradient sensing in yeast. *Nature* **446:** 46–51.
Pereira PS, Jones NC. 2001. The RGS domain-containing fission yeast protein, Rgs1p, regulates pheromone signalling and is required for mating. *Genes Cells* **6:** 789–802.
Petersen J, Weilguny D, Egel R, Nielsen O. 1995. Characterization of fus1 of *Schizosaccharomyces pombe*: a developmentally controlled function needed for conjugation. *Mol Cell Biol* **15:** 3697–3707.
Philips J, Herskowitz I. 1997. Osmotic balance regulates cell fusion during mating in *Saccharomyces cerevisiae*. *J Cell Biol* **138:** 961–974.
Poritz MA, Malmstrom S, Kim MK, Rossmeissl PJ, Kamb A. 2001. Graded mode of transcriptional induction in yeast pheromone signalling revealed by single-cell analysis. *Yeast* **18:** 1331–1338.
Read ND, Fleissner A, Roca MG, Glass NL. 2010. Hyphal fusion. In *Cellular and molecular biology of filamentous fungi (ed.* Borkovich KA, Ebbole DJ), pp. 260–273. American Society of Microbiology, Washington DC.
Rothbauer U, Zolghadr K, Muyldermans S, Schepers A, Cardoso MC, Leonhardt H. 2008. A versatile nanotrap for biochemical and functional studies with fluorescent fusion proteins. *Mol Cell Proteomics* **7:** 282–289.
Rothbauer U, Zolghadr K, Tillib S, Nowak D, Schermelleh L, Gahl A, Backmann N, Conrath K, Muyldermans S, Cardoso MC, et al. 2006. Targeting and tracing antigens in live cells with fluorescent nanobodies. *Nat Methods* **3:** 887–889.
Seike T, Nakamura T, Shimoda C. 2013. Distal and proximal actions of peptide pheromone M-factor control different conjugation steps in fission yeast. *PLoS One* **8:** e69491.
Tanaka K, Davey J, Imai Y, Yamamoto M. 1993. *Schizosaccharomyces pombe* map3^{+} encodes the putative M-factor receptor. *Mol Cell Biol* **13:** 80–88.
Vjestica A, Merlini L, Dudin O, Bendezu FO, Martin SG. 2016. Microscopy of fission yeast sexual lifecycle. *J Vis Exp*.
Watson P, Davis K, Didmon M, Broad P, Davey J. 1999. An RGS protein regulates the pheromone response in the fission yeast *Schizosaccharomyces pombe*. *Mol Microbiol* **33:** 623–634.
West C, Hanyaloglu AC. 2015. Minireview: spatial programming of G protein-coupled receptor activity: decoding signaling in health and disease. *Mol Endocrinol* **29:** 1095–1106.
Xu HP, White M, Marcus S, Wigler M. 1994. Concerted action of RAS and G proteins in the sexual response pathways of *Schizosaccharomyces pombe*. *Mol Cell Biol* **14:** 50–58.
Yi K, Rubinstein B, Li R. 2013. Symmetry breaking and polarity establishment during mouse oocyte maturation. *Philos Trans R Soc Lond B Biol Sci* **368:** 20130002.